Optical Fiber Technology 46 (2018) 15–23

Contents lists available at ScienceDirect

Optical Fiber Technology

journal homepage: www.elsevier.com/locate/yofte

Comparison of DSP-based TDMA and FDMA channel aggregation techniques in mobile fronthauling

Befekadu Mengesha[a,*], Stefano Straullu[b], Pablo Torres-Ferrera[a], Roberto Gaudino[a]

[a] Politecnico di Torino, C.so Duca degli Abruzzi 24, 10129 Torino, Italy
[b] Istituto Superiore Mario Boella, 10138 Torino, Italy

A B S T R A C T

Cloud Radio Access Network (C-RAN) is perceived as a future essential technology to satisfy the ever-increasing demand of mobile data traffic. Considerable research efforts are expending in the optimization of C-RAN architecture. In this paper, we perform a comparison of two DSP-based fronthauling techniques for aggregation of radio waveforms: time division multiple access (TDMA) and frequency division multiple access (FDMA), in terms of error vector magnitude (EVM), spectral bandwidth efficiency and digital signal processing (DSP) complexity as a performance metrics. The two techniques are compared by means of simulation and validated experimentally on an intensity modulation and direct detection (IM-DD) optical fronthaul link capable of aggregating 48 and 96 LTE-A (20 MHz) channels. Moreover, we made simulation comparison on 24 (100 MHz) new radio (NR) waveforms which will be used in the upcoming 5G applications. We reveal that there is ~50% and ~20% spectral efficiency gain by TDMA aggregation on LTE-A and NR waveforms respectively. Hence TDMA gives slightly better performance in the case of 96 LTE-A channels which is attributed to slightly better linearity over the optical channel frequency response for larger number of channel. In addition, we show that TDMA is more efficient in terms of complexity than FDMA system that requires an additional pre-emphasis technique to equalize the overall per channel performance.

1. Introduction

The explosive growth of mobile data traffic demand in radio cellular networks have unceasingly driven the development of higher-speed wireless and wired technology. The 4G LTE-A network standards are currently being deployed worldwide, while the vendors and telecom operators are working towards the next 5G network standardization. It is perceived that mobile network future expansion required to support higher capacity will necessarily require less capital expenditure (CAPEX) and operational expenditure (OPEX) and therefore a set of novel radio access technologies. The emerging enabling technology named as Cloud Radio Access Network (C-RAN) [1,2] architecture is proposed to support the upcoming next-generation mobile technologies, enhancing RAN performance, by centralizing some of the base-band units (BBUs) physical layer processing and higher layer functionalities at the Central Office, and supervise remote radio heads (RRHs) cooperatively. So that the hardware function of RRHs become very simple. The transport of native radio signals over optical fibers, indicated as “fronthauling” by many authors, is regarded as a crucial network segment inside the global C-RAN scenario. Two categories of mobile fronthauling approaches, named as “digitized radio over fiber” (D-RoF, some authors claim that only this approach can be correctly indicated as “fronthauling”) and “analog radio over fiber” (A-RoF, for which some authors prefer to avoid the term fronthauling, talking only of “distributed antenna system”) are currently under consideration [3,4]. The most common fronthauling interfaces in today’s D-RoF are the Common Public Radio Interface (CPRI) [5] and Open Base Station Architecture Initiative (OBSAI) [6]. CPRI is widely used in today’s fronthauling architectures; however, the signal transmission of quantized IQ (In phase and quadrature) samples via CPRI requires very high aggregated bit rate on the optical link. For example, a transport of an 8x8 MIMO 3-sector 2x20 MHz LTE macro cell with 48 (20 MHz) long-term evolution advanced (LTE-A) radio waveforms requires a CPRI data rate of 1.2288 Gb/s per each 20 MHz radio signal, resulting an overall aggregated bit rate of 59 Gbps [4] which is costly and impractical to realize for massive MIMO and 5G applications.

A-RoF is currently being studied for mitigating the huge bandwidth provisioning of CPRI. It is a technique of aggregating massive amounts of native radio waveforms on a single wavelength through a more traditional analog radio over fiber approach [7–11].

In this paper, we analyze the performance of two variants of the A-RoF architecture, commonly indicated as “DSP-based channel aggregation”, namely TDMA [10] and FDMA [11] aggregation techniques. These alternatives are aimed to transport in parallel many radio waveforms (channels) on the same fiber. The key goal of our paper is to investigate the bottom-line physical layer performance of the two approaches. Particularly, we focus on determining which of the two gives the lowest error vector magnitude (EVM) [12], better spectral efficiency

* Corresponding author.
E-mail address: befekadu.mengesha@polito.it (B. Mengesha).

https://doi.org/10.1016/j.yofte.2018.08.022
Received 11 June 2018; Received in revised form 8 August 2018; Accepted 29 August 2018

(since bandwidth become the bottleneck in 4G and 5G new radio systems) and less DSP complexity for a given set of aggregated waveforms on the same optoelectronic transceivers and link.

To this end, we first developed simulation of a realistic bandlimited intensity modulation and direct detection (IM-DD) optical link with external Mach-Zehnder modulation and Avalanche-Photodiode (APD) based receivers. Despite of being more expensive and introducing excess noise with respect to the conventional PIN photodiodes, APDs provide avalanche gain which can yield high overall SNR, lowering the EVM [13] required for the high speed fronthauling architecture studied in this paper [14,15]. Instead, PIN-based photodiodes are suitable for point-to-point links that requires lower sensitivity [16].

Finally, but most importantly, we performed an experimental campaign to demonstrate our obtained simulation results.

The work presented in this paper focuses on the transport of native radio LTE-A signal (specifically on many 20 MHz channels) and advanced 5G new radio NR (100 MHz) signals, while the transport of control information is not considered.

The paper is organized as follows: Section 2 describes the simulation details of the realistic IM-DD model and experimental setups for the two aggregation schemes and the DSP blocks common to simulation and experiment. Section 3 introduces and elaborates the simulation results obtained by the emulation of realistic IM-DD optical link and the experimental results as well as the simulation analysis on the impact of chromatic dispersion. Section 4 concludes the paper by summarizing our main outcomes.

2. Simulation and experimental setup

The details of the simulation setup used to emulate the realistic IM-DD optical link and the experimental setup which validates our simulation are elaborated in the following sub-sections. Moreover, the DSP blocks which are common to both simulation and experimental approaches are also outlined in this section.

2.1. Experimental setup

The experimental setup of the IM-DD optical link is shown in Fig. 1. At the transmitter side we used an arbitrary waveform generator (AWG) capable of processing offline generated DSP waveforms based on either TDMA or FDMA aggregation schemes. It is used as digital-to-analog converter (DAC) in our fronthauling implementation with a sampling rate constrained to 12-GSa/s and vertical resolution of 10 bits. Electrical driver is used to drive the electrical domain signal $x_c(t)$ to the MZM radio frequency (RF) input. An external MZM is used to modulate the continuous wave (CW) carrier, generated by the external cavity laser source at central wavelengthλ = 1550.92 nm. The DC bias of MZM is set to operate the modulator in its quadrature point [17]. The instantaneous optical signal at the output of the MZM is then amplified by an erbium doped fiber amplifier (EDFA), to obtain an average transmitted output optical power ($\bar{P}_{Tx}$) of + 9 dBm [17]. We point out that this power level is not particularly high in the framework of NG-PON2 solutions (some implementation of time and wavelength division multiplexed passive optical networks (TWDM-PON) allows launched power of around +9 dBm and even more for video-overly over PON, which can transmit much higher power level). The EDFA in our experiment is inserted only to counteract the loss of the used external modulator, but we verified that its noise level is negligible in the condition of use, so that noise-wise the experiments are still limited by the receiver noise. The optical output signal is launched into 25 km of single mode fiber (SMF). Variable optical attenuator (VOA) is used to emulate the high overall Optical Distribution Network (ODN) loss typical in a PON link.

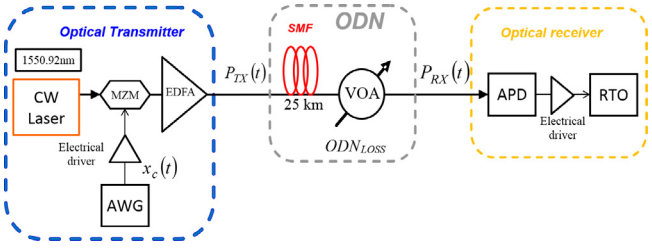

Fig.1. Experimental setup.

At the receiver side, a 10 Gbps APD + TIA (LabBuddy model from Discovery Semiconductors) is used to convert the received optical power into an electrical current. The output current from the APD is then stored on a real time oscilloscope (RTO) characterized by a sampling rate of 40 GSa/s, 10 GHz analogue bandwidth and vertical resolution of 8 bits. The RTO is used as an analogue-to-digital converter (ADC) and stores the samples which are then processed offline to evaluate the performance metrics.

2.2. Simulation setup

The simulation setup of the realistic IM-DD optical model is shown in Fig. 2. The assumptions of the model are described below.

At the transmitter side, a classical nonlinear external MZM model is used with the following parameters: static extinction ratio (ER) = 27.8 dB, insertion loss (IL) = 1.8 dB, V_π radio frequency (RF) electrode voltage = 3.0 V, direct current (DC) bias voltage = $V_\pi/2$ V and modulation index M = 100%. The CW carrier is assumed to be phase and amplitude noiseless operating at wavelength 1550.92 nm. The DAC is realized by vertical resolution of 10 bits. The optical channel transfer function (CHTF) block is simulated considering the optical signal propagation into standard single mode fiber (SSMF) specified by chromatic dispersion (CD) coefficient CD = 17 ps/nm·km and span length L = 25 km. The optical channel frequency response is modelled using 4th order Bessel filter having a 3-dB bandwidth of 2.5 GHz, which was a best-effort fitting of the end-to-end electrical-to-electrical transfer function experimentally measured in the laboratory.

At the receiver side, we modelled the APD assuming that it is constrained by noise contribution that arises from Gaussian amplified shot noise, receiver electrical thermal noise in the receiver circuitry and dark current noise that are independent and identically distributed [18]. Usually, the most relevant part is the amplified shot noise, which we estimated as flat across the full system bandwidth, so that its variance on a channel bandwidth w_{ch} can be estimated as:

$$\sigma_{sn}^2 = 2qM\,F_{APD}\rho\bar{P}_{Rx}w_{ch} \quad (1)$$

where q is the charge of an electron and F_{APD} is the excess noise factor, M is the maximum APD gain, ρ is unity gain responsivity at wavelength 1550.92 nm and $\bar{P}_{Rx}$ is received optical power . The electrical thermal noise variance is:

$$\sigma_\tau^2 = S_{th}^2 \cdot w_{ch} \quad (2)$$

Where S_{th} is input-referred thermal current. The following specification are used to model the APD: $S_{th} = 11pA/\sqrt{Hz}$, $F_{APD} = 5.5$, $M = 7$ and$\rho = 0.875\,[A/W]$. When considering a PIN receiver, we assumed $M = 1$ and $F_{APD} = 1$.

ADC is simulated by 8 quantization bits. The DSP transmitter and receiver sections of the two aggregation schemes are discussed in the following sub-section.

2.3. DSP setup

The transmitter and receiver DSP blocks are shown in Fig. 3 (for FDMA) and Fig. 4 (for TDMA). We generated an emulation of N_{ch} = 48 and 96 LTE-A (20 MHz) waveforms, each made by an OFDM modulation on 2048 points sampled at 30.72 MHz, using 64-QAM modulation format for both aggregation approaches. This modulation is one of the

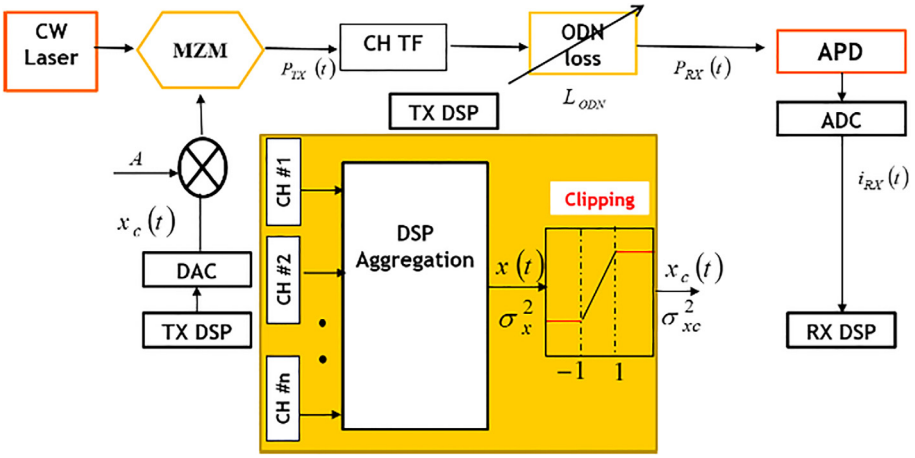

Fig. 2. Simulation setup of IM-DD optical model, consisting of continuous wave (CW) laser, optical modulator, transmitter digital signal processing (TX DSP), digital-to-analogue-converter (DAC), optical channel transfer function (CH TF), optical distribution network loss (ODN loss), avalanche photodetector (APD), analogue-to-digital-converter (ADC) and receiver digital signal processing.

options of the LTE ETSI standard, and occupies a 20 MHz band, carrying approximately 120 Mbit/s gross per channel. We also emulated aggregation of 24 NR (100 MHz) wide bandwidth waveforms which will be proposed as a candidate technology for International Mobile Telecommunications IMT-2020, each made by 4096-point OFDM using subcarrier spacing (SCs) of 30 kHz sampled at 122.88 MSa/s [19]. The aggregated signal, either by FDMA or TDMA at the transmitter DSP output are resampled to fit AWG sampling frequency of 12 GSa/s.

The signal evolution in the FDMA DSP was already mentioned in [10] and the resulting spectrum for 48 LTE-A channels is shown in Fig. 5. We also briefly summarize the signal flows of the TDMA case [11], where, as shown in Fig. 4, the following operation are performed:

- LTE-A or NR complex waveforms are first aggregated in the time domain by simply time-interleaving each time sample;
- the aggregated complex baseband signal is then up-sampled to the required DAC sampling frequency (including an image rejection filtering);
- DSP-based IQ frequency up conversion is used to obtain a real output signal;

hard clipping is finally introduced with the desired clipping ratio. The resulting spectrum for 48 LTE-A channels is shown in Fig. 6.

For the TDMA DSP receiver section, the APD output signal is processed as follows:

- it is down-converted and down-sampled to baseband and then filtered to prevent aliasing;
- the resulting baseband signal is then TDM de-aggregated;
- one tap equalization is used to equalize the channel impairments on the de-aggregated waveforms; the EVM performance is finally estimated on the decoded waveforms.

We present in Fig. 7 an example of the resulting probability density function (pdf) of the aggregated outputs of TDMA and FDMA signal obtained by simulation of 96 LTE-A channels (N_{ch}). We also superimpose a Gaussian pdf with the same variance. The three curves are almost completely superimposed, showing that both the FDMA and TDMA aggregated signals are well approximated by a Gaussian distribution, a result that arises from the central limit theorem (we are aggregating N_{ch} statistically independent OFDM signals, each of which is already Gaussian-like).

3. Results and discussion

The simulated electrical spectrum of 96 (20 MHz) aggregated LTE-A waveforms considering a flat channel is shown in Fig. 8. The blue curve indicates the aggregated TDMA channels, whereas the red curve shows the corresponding FDMA channels. As shown in the figure, the spectral bandwidth occupancy of FDMA is greater than the TDMA for the following reasons: the overall signal bandwidth occupied by the aggregated FDMA channel is $B_{FDMA} = N_{ch} \cdot F_s$, where F_s is the sampling frequency of single LTE-A waveform. For example, for $N_{ch} = 96$ waveforms and $F_s = 30.72$ MHz, the spectral occupancy is approximately 3 GHz. In contrast, the bandwidth occupied by TDMA signal is $B_{TDMA} = N_{ch} \cdot w_{ch}$. For example, considering the same number of

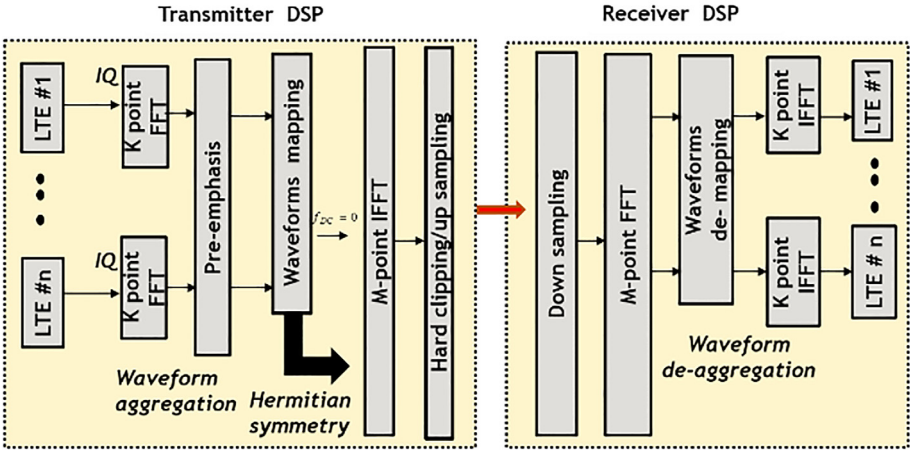

Fig.3. FDMA DSP setup (where k = 16, M: depends on the number of aggregated signals, for instant M = 2048 for 48 channels).

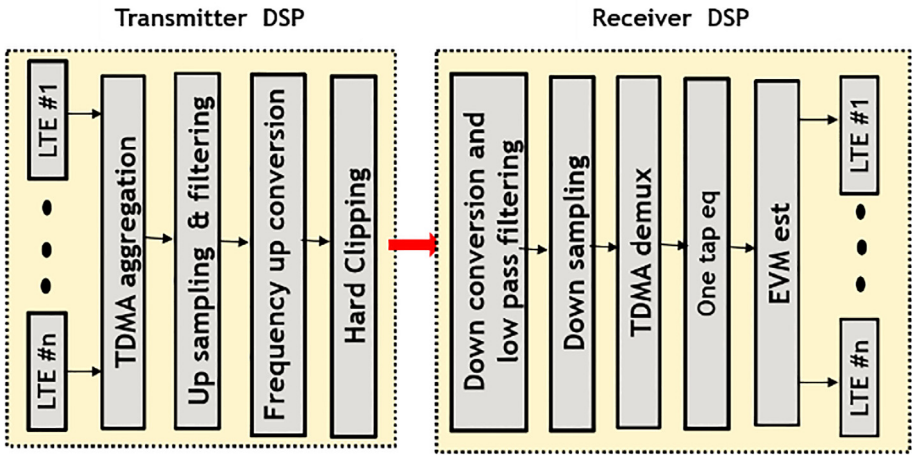

Fig.4. TDMA DSP setup.

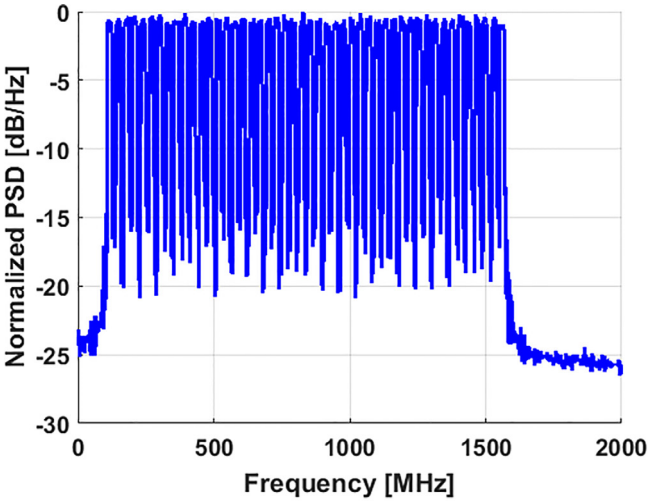

(a)

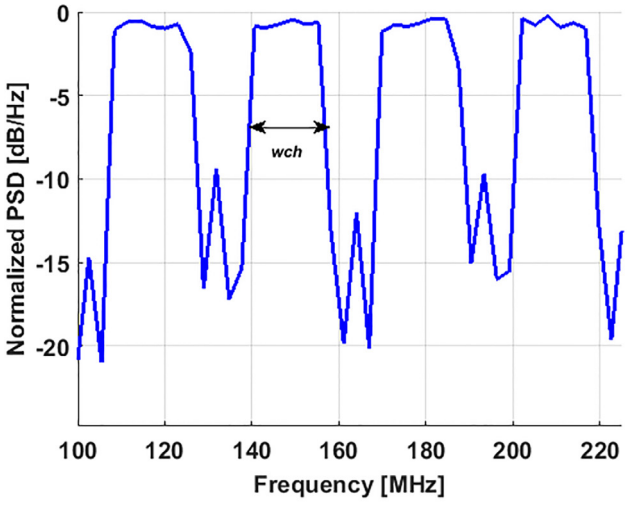

(b)

Fig. 5. Power spectral density of simulated 48 aggregated FDMA signal: a) Full spectrum b) Zooming in the first 4 FDMA channels.

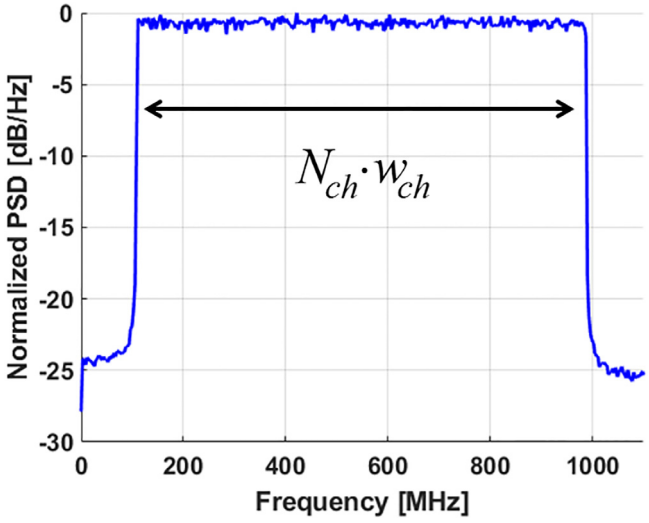

Fig. 6. Power spectral density of simulated 48 aggregated TDMA signal.

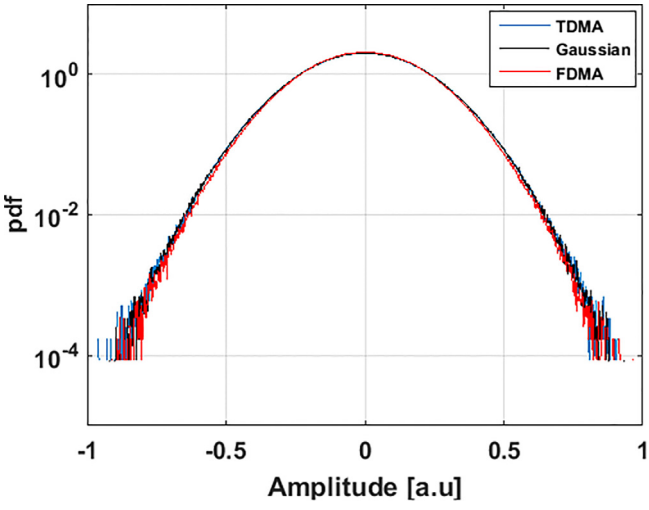

Fig.7. PDF of the aggregated output of the TDMA and FDMA signal superimposed with Gaussian distribution.

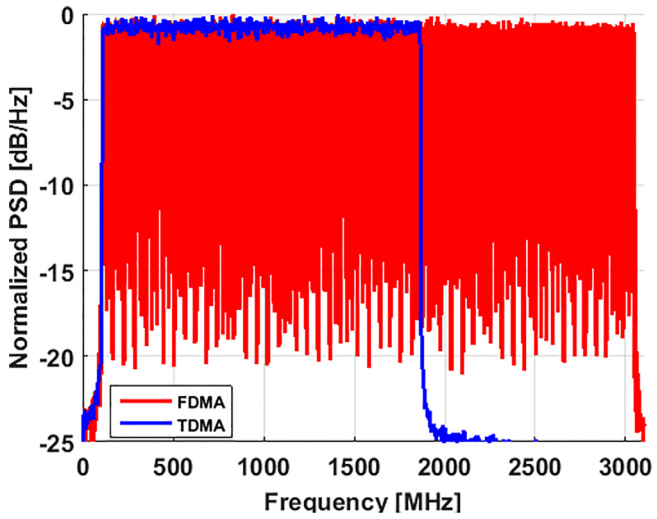

Fig. 8. Electrical spectrum of TDMA and FDMA signal realized under flat optical channel response (simulated) for 96 (20 MHz) LTE-A channels.

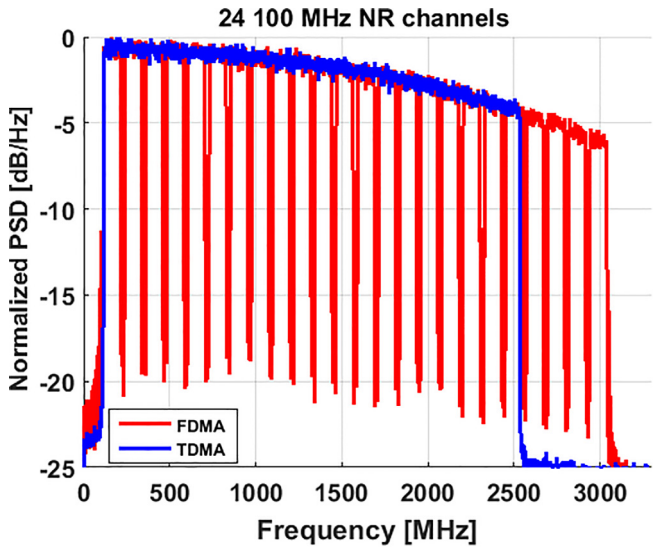

Fig. 9. Electrical spectrum of TDMA and FDMA signal realized under simulation of realistic IM-DD link for 24 (100 MHz) NR channels.

channels $N_{ch} = 96$ and single LTE-A waveform bandwidth $w_{ch} = 20$ MHz, the bandwidth occupied by aggregated TDMA signal is approximately 2 GHz, hence the spectrum efficiency is improved by 50% and at least 6 GSa/s DAC is required in the case of FDMA , while only 4 GSa/s DAC is required in TDMA scheme. Similarly, the electrical spectrum of 24 (100 MHz) NR waveforms simulated under the assumption of realistic IM-DD link is shown in Fig. 9. The blue curve indicates TDMA whereas the red curve indicates FDMA aggregation. The bandwidth occupied by FDMA is $B_{FDMA} = N_{ch} \cdot F_s$ where $N_{ch} = 24$ and $F_s = 122.88$ MHz, spectral bandwidth occupation is approximately 3 GHz. The bandwidth occupied by TDMA is $B_{TDMA} = N_{ch} \cdot w_{ch}$ where $w_{ch} = 100$ MHz, is approximately 2.5 GHz. Therefore, the spectrum bandwidth efficiency is improved by ~20% with TDMA. This verifies that the spectral efficiency gain using TDMA is more significant in the case of LTE-A aggregation than the NR waveforms.

The electrical spectrum of the received signals obtained by both simulation and experiment for 48 and 96 LTE-A channels are presented in Fig. 10 and in Fig. 11, respectively. As shown in Fig. 10, the optical channel response on 48 channels is almost flat for both TDMA (Fig. 10(a)) and FDMA (Fig. 10(b)) signals, whereas in case of 96 LTE-A channels, the optical channel response shows significant frequency roll-

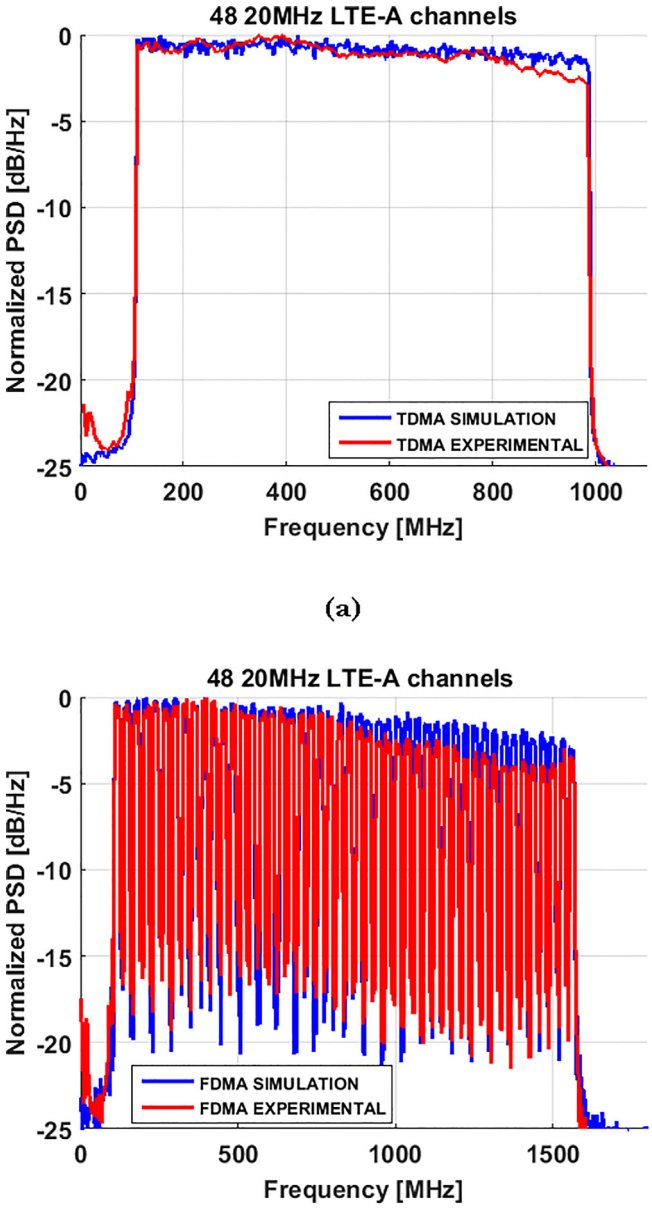

Fig. 10. Received signal spectrum of 48 (20 MHz) LTE-A channels obtained by simulation and experiment, (a) TDMA and (b) FDMA.

off toward higher frequency as shown in Fig. 11. The slight difference between simulation and experiment is attributed to intermodulation distortion (IMD) caused by the nonlinear optoelectronic devices used on the experimental investigation which were not considered in the simulation as well as the APD's simulation flat noise consideration over the system bandwidth. As shown in Figs. 10(a) and 11(a), distortion effect is more significant in the FDMA scheme.

Besides bandwidth occupation and frequency roll-off, a key parameter for the considered systems is the degree of clipping: under the convention we have used to define the parameter R_{cl} as

$$R_{cl} = 1/\sigma_x^2 \tag{3}$$

where σ_x^2 is the variance of the signal to be clipped. Small values of R_{cl} (i.e. strong hard clipping) give rise to a large clipping distortion, whereas large values of R_{cl} reduce clipping distortion but generate a small signal that is thus less resilient to receiver noise. We then look for

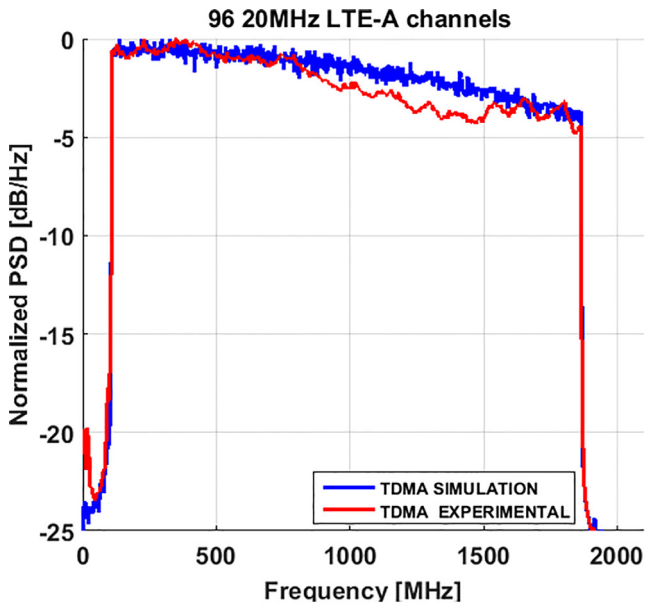

Fig. 11. Received signal spectrum of 96 (20 MHz) LTE-A channels obtained by simulation and experiment, (a) TDMA and (b) FDMA.

the optimum clipping R_{cl} for both aggregation approaches with different number of channels. The clipping ratio R_{cl} vs. *EVM (*computed as the mean value of the EVM of all channels) for 48 channels at ODN loss of 31 dB (a typical target value for PON access networks) is shown in Fig. 12. The blue pentagram with dot-dashed line curve is for TDMA and the red pentagram is used for FDMA. FDMA performance is evaluated by applying pre-emphasis, a technique used to equalize the EVM per channel over frequency. The pre-emphasis method used consists on multiplying each waveform by a scaling factor (a set of globally optimized coefficients) which in turns minimize maximum EVM along the whole set of channels (for an extensive study on frequency pre-emphasis options applied on FDMA, please refer to our previous investigation [20]). As depicted in Fig. 12, simulation and experimental results are consistent in TDMA approach, whereas the slight difference in the case of FDMA can be associated to the significant IMD justified by the mismatch of the profile of the frequency response of the optical

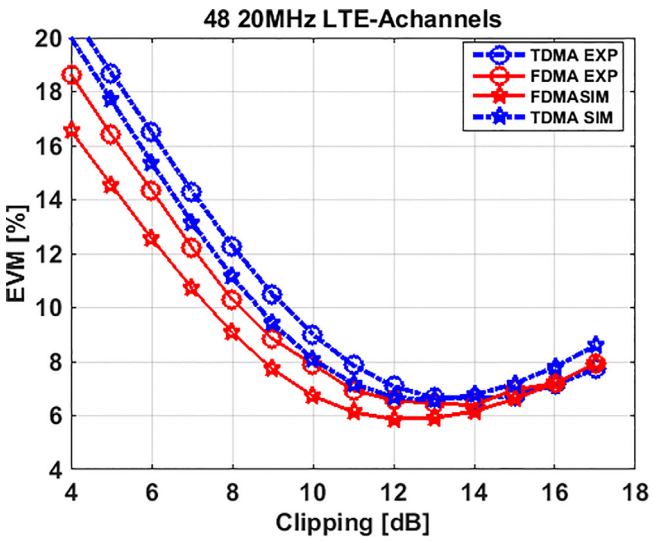

Fig. 12. Clipping optimization for 48 (20 MHz) LTE-A channels at 31 dB ODN loss.

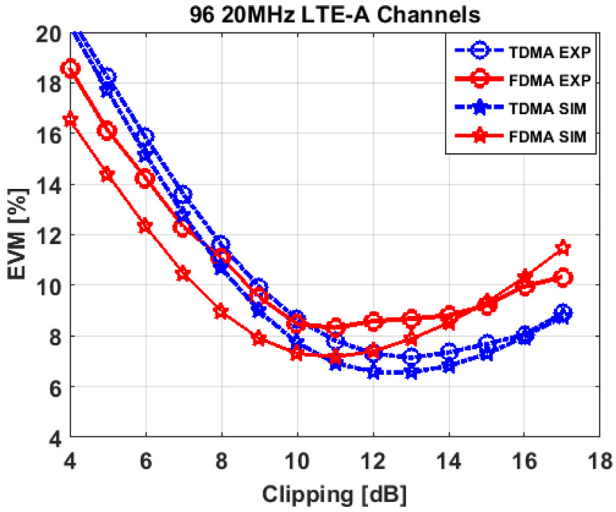

Fig. 13. Clipping optimization for 96 (20 MHz) LTE-A channels at 29 dB ODN loss.

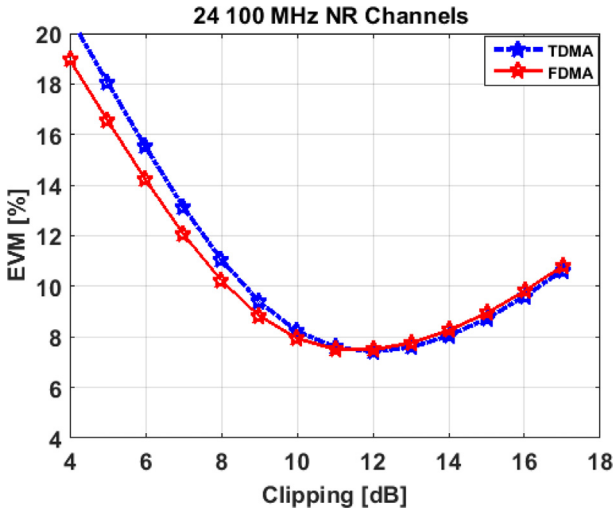

Fig. 14. Clipping optimization for 24 (100 MHz) NR channels at 29 dB ODN loss.

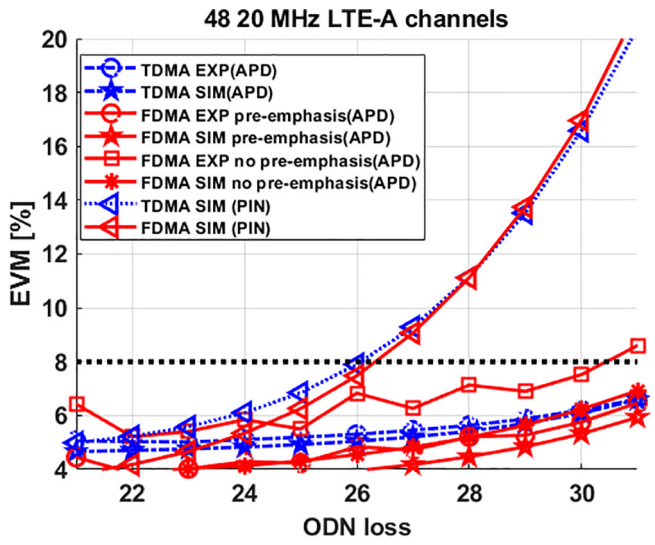

Fig. 15. Mean EVM vs. ODN loss for 48 (20 MHz) LTE-A channels clipped at 13 dB for both TDMA and FDMA systems.

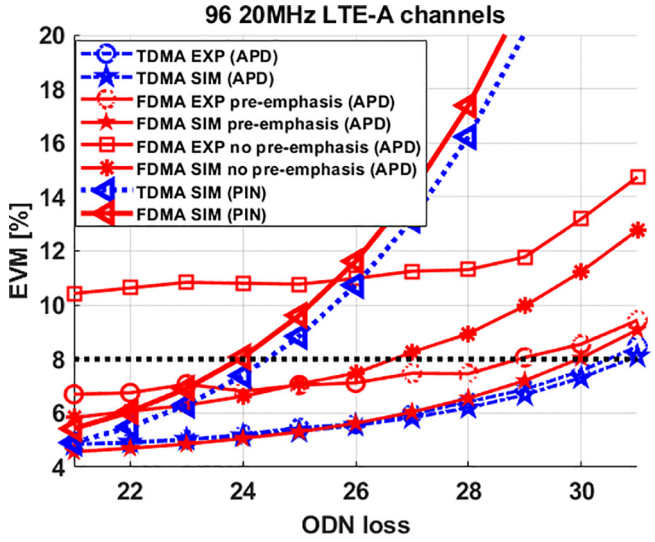

Fig. 16. Mean EVM vs. ODN loss for 96 (20 MHz) LTE-A channels clipped at 13 dB for TDMA and 11 dB for FDMA.

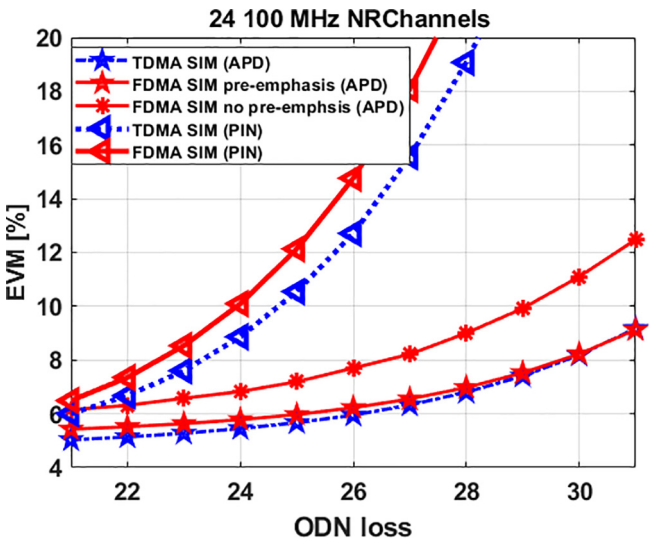

Fig. 17. Mean EVM vs. ODN loss for 24 (100 MHz) NR channels clipped at 12 dB for both TDMA and FDMA.

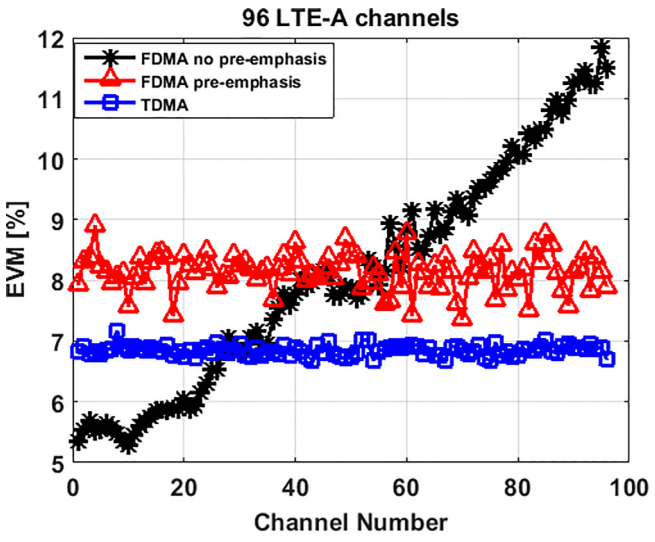

Fig. 18. Per channel EVM in case of 96 (20 MHz) LTE-A channels at 29 dB ODN loss at 13 dB clipping ratio for TDMA and 11 dB for FDMA.

channel shown in Fig. 10(b). The optimum clipping ratio (level) for both systems, in simulation and experiments, is obtained at R_{cl} of 13 dB. The clipping ratio R_{cl} vs. *EVM (mean)* for 96 LTE-A channels at an ODN loss of 29 dB is presented in Fig. 13, using the same notation as in Fig. 12. The difference in the results between the simulation and experiment is due to IMD effect present on the experiment. The optimum clipping ratio (level) for TDMA is obtained at R_{cl} of 13 dB and for FDMA at R_{cl} of 11 dB, both by simulation and experiment. The R_{cl} vs. *EVM* obtained by simulation of 24 NR channel is depicted in Fig. 14. The optimum clipping ratio for both aggregation scheme is obtainedR_{cl} = 12 dB.

The EVM (mean) as a function of ODN loss is then reported in Figs. 15 and 16 for 48 and 96 LTE-A channels, respectively. The same notation is followed as in Fig. 12. In addition, the star and square markers are used to indicate the worst channel EVM performance obtained by simulations and experiments, respectively, when no pre-emphasis is applied. The EVM performance of the two systems on 48 LTE-A channels is almost similar when the pre-emphasis is applied, which is attributed to the flat response of the optical channel. However, the performance toward higher channels is slightly degraded without pre-emphasis when the frequency response of the optical channel shows significant roll-off towards high frequencies as in the case of 96 LTE-A channels as shown in Fig. 11. The EVM (mean) as a function of ODN loss obtained by simulation of 24 (100 MHz) NR channels is shown in Fig. 17. The EVM performance of the two systems on 24 NR channels shows similar results when pre-emphasis is applied, however the performance of FDMA is significantly degraded towards higher frequency channels without pre-emphasis and therefore pre-emphasis is strictly necessary. The simulation results on the impact of using PIN photodiode receiver on the EVM performance is also presented on Figs. 15–17. The blue triangular dot line curve is used for TDMA with PIN receiver and the red triangular solid line curve is used for FDMA pre-emphasis with PIN receiver. The EVM = 8% target (presented on the figures with black dot line) for 64 QAM modulation format specified in 3GPP-TS recommendation is achieved up to 26 dB ODN loss with PIN and more than 31 dB ODN loss by using APD receiver for the case of 48 LTE-A waveforms as shown in Fig. 15, at 24 dB ODN loss for PIN receiver and 30 dB ODN loss with APD for the case of 96 LTE-A waveforms as shown in Fig. 16 and at 23 dB ODN loss with PIN receiver and 30 dB with APD receiver for the case of 24 (100 MHz) NR as shown in

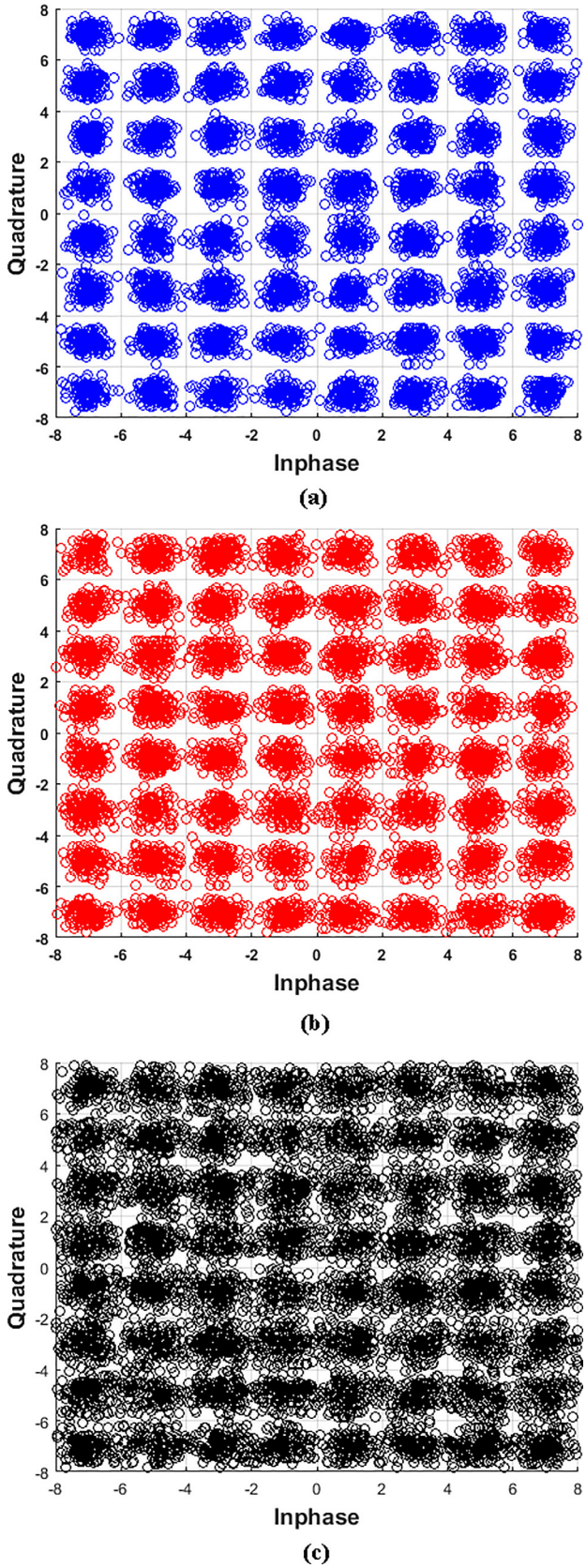

Fig. 19. The decoded constellation plot of the 96th channel at 29 dB ODN loss (a) TDMA at 13 dB clipping ratio, (b) FDMA with pre-emphasis at 11 dB clipping ratio, (c) FDMA without pre-emphasis at 11 dB clipping ratio.

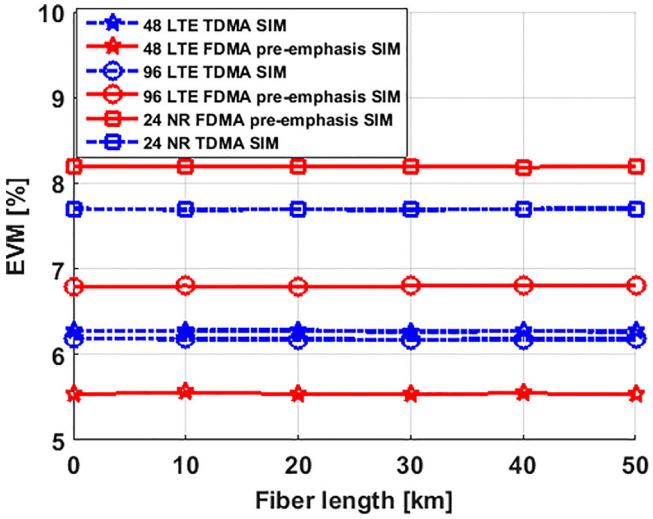

Fig. 20. Impact of chromatic dispersion on the EVM performance of 48 20 MHz LTE-A channels at 31 dB ODN loss, 96 20 MHz LTE-A channels at 29 dB ODN loss and 24 100 MHz NR channels at 29 dB ODN loss.

Fig. 17. In all the three cases, PIN receiver have lower performance, and in particular they cannot be used for the higher considered ODN path losses, specifically at 29 dB ODN loss required by PON standards. PIN receivers can anyway be interesting for point-to-point fronthauling solutions (i.e., not in PON). In the following, we have decided to focus on APD receiver structures, since the paper is actually targeting PON solutions.

The EVM performance on each channel for the 96 LTE-A channels obtained by experiment at 29 dB ODN loss and optimum clipping factor is presented in Fig. 18. Apart from the better performance, TDMA gives uniform EVM on the overall channels. In contrast, the FDMA performance towards higher number of channels is severely degraded without transmitter pre-emphasis, demonstrating that pre-emphasis technique is a must in the FDMA case. The decoded constellation of the 96th (worst) LTE channel for the three cases is finally shown in Fig. 19. Fig. 19(a) shows the TDMA received signal constellation at EVM = 7%, Fig. 19(b) shows the FDMA pre-compensated (pre-emphasis) received signal constellation at EVM = 8% and Fig. 19(c) depicts the FDMA without pre-emphasis received signal constellation at EVM = 12%.

We analyzed the impact of chromatic dispersion on the link performance of the two aggregation schemes basing on the simulation results obtained for 48 (20 MHz) LTE-A, 96 (20 MHz) LTE-A and 24 (100 MHz) NR channels using APD receiver shown in Fig. 1. The EVM corresponding to optimum clipping level of the three cases as a function of SSMF single span length of up to 50 km is reported in Fig. 20. The dash-dot line (blue color) is used for TDMA and the solid line (red color) is used to indicate FDMA with pre-emphasis simulation results. Moreover, pentagram marker is used for 48 LTE channels at 31 dB ODN loss, the circle marker is used to show 96 LTE channels at 29 dB ODN loss and the square marker is used to show 24 NR channels at 29 dB ODN loss. We verified that chromatic dispersion has negligible penalty on the system EVM performance up to 50 km of SSMF.

4. Comments and conclusion

The comparison between TDMA and FDMA aggregation approaches on LTE-A and wideband NR waveforms showed that TDMA gives significant spectral efficiency gain on 4G LTE-A systems and 5G wideband NR applications than FDMA solution, which in turn leads to slight EVM performance gain. Moreover, when the optical frequency response is relevant towards higher frequency channels as in the case of 96 LTE-A and 24 NR, FDMA requires pre-emphasis (pre-compensation) at the transmitter side to give equalized EVM performance over the whole

channels. Hence, the DSP complexity of FDMA aggregation approach is increased.

Acknowledgment

This work was carried out under the PhotoNext initiative at Politecnico di Torino, Italy (www.photonext.polito.it).

References

[1] A. Checko, H.L. Christiansen, Y. Yan, L. Scolari, G. Kardaras, M.S. Berger, L. Dittman, Cloud RAN for mobile networks—a technology overview, IEEE Commun. Surv. Tutorials. 17 (1) (2015) 405–426.
[2] K Tanaka, A. Agata, Next-generation optical access for CRAN, in: Optical Fiber Communication conf. (OFC), 2015, paper Tu2E.1.
[3] Radio-over-fiber (ROF) technologies and their applications, ITU-T-G-Series Recommendations—Supplement 55, 2015.
[4] D.A.A. Mello, A.N. Barreto, F.A. Barbosa, C. Osorio, M. Fiorani, P. Monti, Spectrally Efficient Fronthaul Architectures for a Cost-Effective 5G C-RAN, in Proc: ICTON, WC2.4, Trento, Italy, 2016.
[5] CPRI Specification V7.0, Oct. 2015 [Online]. Available: http://www.cpri.info/downloads/CPRI_v_7_0_2015-10-09.pdf.
[6] OBSAI Specification, 2013. [Online]. Available: www.obsai.com.
[7] A. Pizzinat, P. Chanclou, F. Saliou, T. Diallo, Things you should know about fronthaul, J. Lightwave Technol. 33 (5) (2015) 1077–1083.
[8] C. Ye, K. Zhang, Q. Chang, Z. Gao, X. Hu, X. Huang, X. Sun, A DSP-Assisted Symbol-Cascade Mobile Fronthaul Solution with Large Capacity and Neat RRHs, in: Proc: ECOC, 2015, paper We4.4.2.
[9] J. Zhang, M. Xu, J. Wang, F. Lu, L. Cheng, Ming Zhu, I. Khalil, J. Yu, G. Chang, Carrier aggregation for MMW inter-RAT and intra-RAT in next generation heterogeneous mobile data network based on optical domain band mapping, in: Proc: ECOC, 2015, paper We4.4.5.
[10] X. Liu, H. Zeng, N. Chand, F. Effenberger, Efficient mobile fronthaul via DSP-based channel aggregation, J. Lightwave Technol. 34 (6) (2015) 1556–1564.
[11] X.L. Zeng, N. Chand Miller, F. Effenberger, CPRI-Compatible efficient mobile fronthalul transmission via equalized TDMA achieving 256 Gb/s CPRI-equvalent data rate in a single 10 GHz-bandwidth IM-DD channel, in: Proc: OFC, 2016, paper W1H.3.
[12] R. Schmogrow, B. Nebandahl, M. Winter, A. Josten, D. Hellerkuss, S. Koeng, J. Meyer, M. Dreschmann, M. Hueber, C. Koos, J. Becker, J. Freude, J. Leuthold, Error vector magnitude as a performance measure for advanced modulation formats, IEEE Photon. Technol. Lett. 24 (2012) 1.
[13] R.A. Shafik, M.S. Rahman, A.R. Islam, On the extended relationships among EVM, BER, and SNR as a performance metrics, in: 4th International Conference on Electrical and Computer Engineering (ICECE) , Dhka, Bangladesh, 2006.
[14] K.M. Johnson, High-speed photodiode signal enhancement at avalanche breakdawn voltage, IEEE Trans. Electron Dev. 12 (1965) 55–63.
[15] S. Xie, X. Zhou, S. Zhang, David J. Thomson, X. Chen, G.T. Reed, J. Shien Ng, C. Hing Tan, InGaAs/AlGaAsSb avalanche photodiode with high gain-bandwidth product, Opt Express 24 (21) (2016) 24242–24247.
[16] E. Vanin, Performance evaluation of intensity modulated optical OFDM system with digital baseband distortion, Opt Express 19 (5) (2011) 4280–4293.
[17] M. Befekadu, S. Straullu, S. Abrate, R. Gaudino, Experimental Optimization of DSP-Aggregated Front-hauling Transmission for up to 4x96 LTE radio waveforms, in: 42th European Conference and Exhibition on Optical Communication (ECOC), Dusseldorf, Germany, 2016.
[18] N.Z. Hakim, E. Bahaa, A. Saleh, M.C. Teich, Signal-to-noise ratio for lightwave systems using avalnche photodiodes, J. Lightwave Technol. 9 (1991) 3.
[19] J. Jeon, NR wide bandwidth operations, IEEE Commun. Mag. 56 (3) (2018) 42–46.
[20] P. Torres-Ferrera, S. Straullu, S. Abrate, R. Gaudino, Upstream and downstream analysis of an optical fronthaul system based on DSP-assisted channel aggregation, J. Optical. Comm. Netw. (JOCN) 9 (12) (2017).